Clays and Clay Minerals, Vol. 69, No. 5:522–532, 2021

COMPOSITE BIODEGRADABLE POLYMERIC MATRIX DOPED WITH HALLOYSITE NANOTUBES FOR THE REPAIR OF BONE DEFECTS IN DOGS

Ekaterina Naumenko[1]*, Elena Zakirova[1], Ivan Guryanov[1], Farida Akhatova[1], Mikhail Sergeev[2], Anastasia Valeeva[2], and Rawil Fakhrullin[1]*

[1]Institute of Fundamental Medicine and Biology, Kazan Federal University, Kreml uramı 18, Kazan, Republic of Tatarstan, Russian Federation 420008

[2]Kazan State Academy of Veterinary Medicine, Siberian Tract, 35, Kazan, Republic of Tatarstan, Russian Federation 420074

Abstract—The use, in veterinary practice, of a three-dimensional biopolymer matrix (based on chitosan, agarose, and gelatin and doped with halloysite nanotubes) as a vehicle for mesenchymal stem cells (MSCs) to repair bone defects is reported here. The nanocomposite, combined with allogenic adipose-derived stem cells, was suitable for the repair of bone defects in dogs when paired with standard surgery involving metal Kirshner wires. The absence of inflammatory reactions to biopolymer matrices with allogenic stem cells was revealed in the case of an animal prone to inflammatory and allergic reactions. In addition, positive dynamics in the fusion of chronic bone defects without rejection reactions was observed after using a biopolymer matrix with MSCs.

Keywords—Adipose-derived mesenchymal stem cells · Biopolymeric scaffolds · Bone restoration · Halloysite nanotubes · Osteoconductive properties

INTRODUCTION

Bone is a solid-state tissue, which contains ~30% matrix, 60% minerals, and 10% water (Athanasiou et al., 2000). Collagen is the main component of bone organic matrix, which is responsible for the tensile strength, whereas the mineral component (calcium phosphate) imparts compressive strength to the bone tissue (Driessens et al., 1978). Despite its relative strength, the bone tissue is susceptible to fracture as a result of trauma or pathological fragility due to deficiency of organic matrix and resorption (Rabie et al., 2000; Cavalcanti et al., 2008). Devices used clinically for bone fixation and repair are fabricated mostly from metals (stainless steel, titanium and its alloys) (Curtis et al., 2005; Goodrich et al., 2012). Metallic devices and implants, due to their non-biodegradable nature, often require additional surgery to remove them from the body, and can cause complications such as allergic reactions and infections (Eppley & Sadove, 1995; Marti et al., 1997; Christensen et al., 2000).

Biodegradable materials for bone repair are preferred because they can be used to fabricate implants and do not require a second surgical invasion for removal (Middleton & Tipton, 2000; Wuisman & Smit, 2006). All materials must support bone-tissue regeneration and repair processes and be compatible with surrounding tissues, provide mechanical strength, and must degrade to non-toxic by-products which are easily removed by the organism (Hutmacher et al., 1996). Biodegradable biopolymers are commonly used in tissue engineering, including bone regeneration, due to their high level of biodegradability and controlled degradation rates which makes them very useful in clinical applications (Ulery et al., 2011; Bertesteanu et al., 2014). The degradation and mechanical properties of polymer materials can be altered by changing their structural composition and fabrication techniques, as well as adding biocompatible nanomaterials as dopants (Naumenko & Fakhrullin, 2017). Halloysite nanotubes (HNTs), which can be used as a dopant in the biopolymer scaffolds, are the hollow version of the halloysite mineral which belongs to the kaolinite group with the following formula: $Al_4[(OH)_8|Si_4O_{10}]x(H_2O)_4$. The linear dimensions of nanotubes vary from 700 nm to 2 μm, the outer diameter is 50 nm, and the inner-cavity diameter is ~15 nm (Abdullayev & Lvov, 2013). As has been demonstrated using various organisms, ranging from bacteria to multicellular organisms, halloysite does not induce any pronounced toxic effect (Fakhrullina et al., 2015; Tarasova et al., 2019). The surface and internal cavity of halloysite nanotubes can be modified in various ways (Yendluri et al., 2017; Fakhrullina et al., 2019; Guryanov et al., 2020; Rozhina et al., 2020). Recently, HNTs were reported as suitable for use in the fabrication of core-shell nanosystens such as metal catalysts (Glotov et al., 2019) as well as protective coatings for hair (Cavallaro et al., 2020). Biopolymer-based composites with added halloysite were fabricated previously and showed a significant increase in mechanical strength when adding even small amounts of HNTs and an increase in the proliferative activity of cells growing on scaffolds (Naumenko et al., 2016).

Osseous wound healing involves the recruitment of MSCs to perform the molecular tasks of bone regeneration. Successful bone repair is possible only in the presence of high titers of MSCs that differentiate into cartilage mass in the avascular region of the wounded tissue. The surrounding matrix repre-

* E-mail address of corresponding authors:
ekaterina.naumenko@gmail.com; kazanbio@gmail.com
DOI: 10.1007/s42860-021-00152-7

This paper belongs to a special issue on 'Clay Minerals in Health Applications'

sents a key component of bone formation or repair (Dimitriou et al., 2011). Numerous materials have been suggested as osteoconductive which support bone formation (Cornell, 1999; Blokhuis, 2014) but the search for a universal material goes on. The development of methods for induction of osteogenesis under conditions of a decrease in local microcirculation and tissue trophism is of particular interest, therefore. The use of tissue-mimicking scaffolds in combination with classical surgical methods is recognized as a promising treatment for fractures of long tubular bones.

MATERIALS AND METHODS

Cell Culture and Morphological Characteristics

Allogenic adipose-derived MSCs were isolated from the donor dog (Alstrup et al., 2019). Cells on the sixth passage for further experiments(Shall et al., 2018; Yang et al., 2018) were cultivated on Minimal Essential Medium Alfa modification (α-MEM) supplemented with 10% fetal bovine serum (PAA Laboratories, Pasching, Austria), 45 U/mL penicillin, and 45 mg/mL of streptomycin (PanEco, Moscow, Russia). For morphology and cytoskeleton visualization, cells were stained with FITC-conjugated phalloidine (Invitrogen, Carlsbad, California, USA) according the manufacturer's recommendations. The cells were examined using a confocal fluorescent microscope, LSM 780 (Carl Zeiss, Oberkochen, Germany); the images were processed using *ZEN* software. The ability of the MSCs to grow on the surface of the porous matrix was estimated using an inverted microscope AxioObserver A1 (Carl Zeiss, Oberkochen, Germany).

Dark-field microscopy images of MSCs were obtained using an Olympus BX51 upright microscope equipped with a CytoViva® enhanced dark-field condenser, fluorite 100× objective and DAGE CCD camera (Akhatova et al., 2018a).

Atomic force microscopy images were collected using a Dimension Icon microscope (Bruker, Billerica, Massachusetts, USA) operating in PeakForce Tapping mode. Cells were imaged using ScanAsyst-Air probes (Bruker, Billerica, Massachusetts, USA) (nominal length 115 μm, tip radius 2 nm, spring constant 0.4 Nm^{-1}). The images were obtained at 512 lines/scan at 0.8–0.9 Hz scan rate and up to 1 nN peak force setpoint. Topography was visualized in height sensor and peak force error channels. The AFM data were processed using *Nanoscope Analysis* v.1.7. software (Bruker, Billerica, MA, USA) (Fakhrullina et al., 2017; Akhatova et al., 2018b).

Imunocytochemical Analysis of ADSC

For immunocytochemical analysis with subsequent determination of the 'stemness' of isolated cells, the following conjugated antibodies were used: CD 44 (Bio Legend, San Diego, CA, № 103028), CD10 (Sorbent, Moscow, Russia), and CD 71 (Sorbent, Moscow, Russia). The cellular monolayer was stained according to the recommendations of the manufacturers. Specimens were observed using a confocal fluorescent microscope – LSM 780 (Carl Zeiss, Oberkochen, Germany); images were processed using *ZEN* software.

Differentiation of MSCs

The ability of the allogenic MSCs to differentiate into specialized cell types was studied using specific staining protocols. Cells of the sixth passage were plated on 12-well plates (30,000 cells/well) and incubated in complete α-MEM growth medium until a monolayer culture was obtained (48 h). Subsequently, cells were incubated with special media to induce differentiation in three directions: osteogenic, adipogenic, and chondrogenic (Cho et al., 2015). The nutrient media were changed twice per week. After 21 days of incubation with differentiating media, the cell cultures were fixed with cooled methanol for 20 min at –20°C, and cytochemical staining was performed. To determine the mineralization (osteogenic differentiation), the von Kossa reaction was used (Meloan & Puchtler, 1985). Briefly, silver nitrate solution (2% (w/v)) was applied on the cells with subsequent incubation for 1 h under bright illumination. To identify the oil droplets in the cells which were incubated in adipogenic differentiation medium, the qualitative reaction for neutral fats with the Sudan III (Sigma-Aldrich, St. Louis, Missouri, USA) dye was used (Lo Furno et al., 2013). Cell nuclei were stained with a solution of hematoxylin. To detect chondrogenic differentiation, the staining for the markers of chondrocytes and the surrounding matrix formation (mucopolysaccharides) was used. Fixed cells were washed with phosphate buffer saline three times for 5 min, stained for 1 h with Alcian Blue (1 g Alcian Blue/100 mL 0.1 M HCl), and then washed with DPBS. During the differentiation process, MSCs cultures were monitored intravitally every 24 h under an inverted AxioObserver A1 microscope (Carl Zeiss, Oberkochen, Germany) using phase-contrast imaging. After specific staining, the specimens were observed under an AxioImager microscope (Carl Zeiss, Oberkochen, Germany) and the images were processed with *ZEN* software.

Fabrication of Porous Nanocomposite Scaffolds

Biopolymeric scaffolds with HNTs were obtained via a freeze-drying technique as described previously (Naumenko et al., 2016). A column 1.5 cm in diameter and 4 cm in height was formed for the implantation. Briefly, 1% gelatine, 1% chitosan, and 2% agarose were dissolved in 1% acetic acid solution with dispersed HNTs (6 wt.%) and incubated at 80°C for 2 h in a water bath. Then the gel was cast into moulds of appropriate shape and frozen at –80°C for 24 h, followed by freeze-drying. Allogenic MSCs (5×10^6–7×10^6) were applied to the scaffold 3 days before the operation and incubated in complete α-MEM with replacement every 24 h.

Fourier-transform Infrared Spectroscopy

Fourier-transform infrared (FTIR) spectra of pure polymers, HNTs, and scaffolds were collected using a Frontier FTIR spectrometer FT-801 (OSTEC FTIR Spectrometer, Moscow, Russia). The measurements were recorded at room temperature in the range between 500 and 4000 cm^{-1} with a spectral resolution of 2 cm^{-1}.

https://doi.org/10.1007/s42860-021-00152-7 Published online by Cambridge University Press

Post-operative Care of the Dog

In the early post-operative period, the following drugs were used:

Ceftriaxone – 1 g twice per day, intramuscularly, for 10 days, to prevent surgical infection. Before administration, a dose of antibiotic was dissolved in 4 mL of 0.5% Novocaine solution;

Nefopan solution – 20 mg/mL, intramuscularly, in a dose of 1 mL, twice per day for 5 days in order to eliminate post-operative pain.

Ethics Approval

The protocol for the present study was approved by the Biomedicine Ethics Expert Committee of Kazan Federal University (protocol #3; May 5th, 2015) under institutional and international ethical guidelines. Injections and care were given, in accord with standard veterinary practice recommendations, by qualified clinicians with additional health and welfare checks and clinical observations.

RESULTS

The research outline and a schematic diagram for fabrication of porous nanostructured scaffolds are illustrated in Fig. 1. Microscopy images of halloysite used as a dopant for the fabrication of nanomodified scaffold material and combined with MSCs for repair of the bone defect are presented in Fig. 2.

The main polymer of the fabricated scaffolds was agarose (2%) whereas the concentration of chitosan and gelatin was 1%. The FTIR spectrum of pure commercial agarose is presented in Fig. 3. The peak positions at 947 and 976 cm^{-1} are present in both the agarose and scaffold+HNTs samples. A subsequent characteristic decrease in the scaffold+HNTs curve along the *y* axis was also observed in the agarose sample. The peaks (C–O stretch) of scaffold+HNTs related to agarose are present in the range between 1100 and 1300 cm^{-1} (Singh et al., 2017), but with a shift in the peak position. At the same time the position of 1149 cm^{-1} in the scaffolds corresponded to the chitosan sample. The general profile of the FTIR spectra of the scaffold was most like that of agarose, related to its prevalence over other polymers. The observed shift in the agarose peaks in

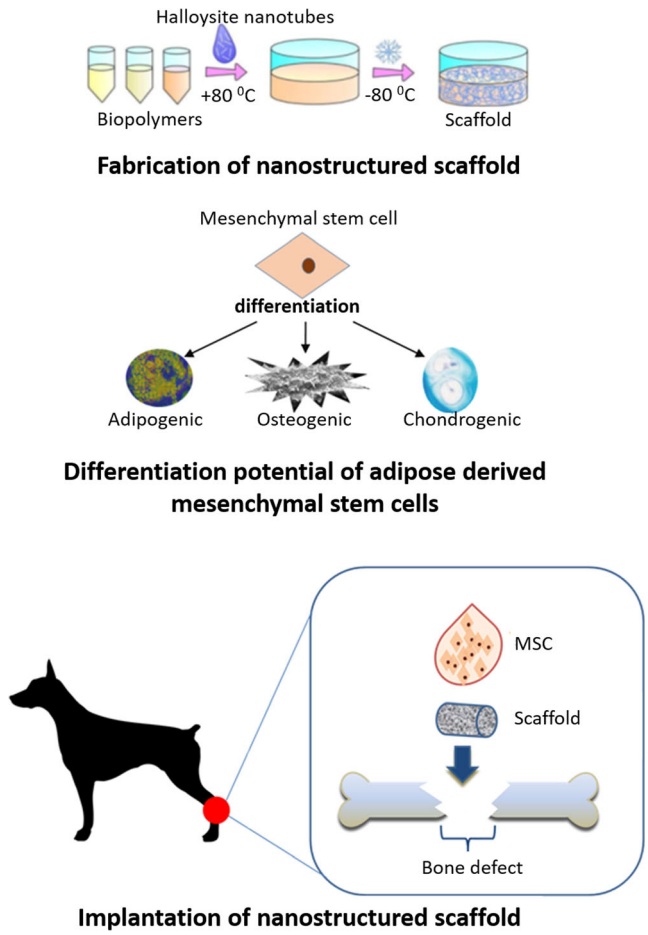

Fig. 1. Sketch demonstrating the fabrication of the scaffold, differentiation of MSCs, and the implantation of scaffold with MSCs in the area of the bone defect

https://doi.org/10.1007/s42860-021-00152-7 Published online by Cambridge University Press

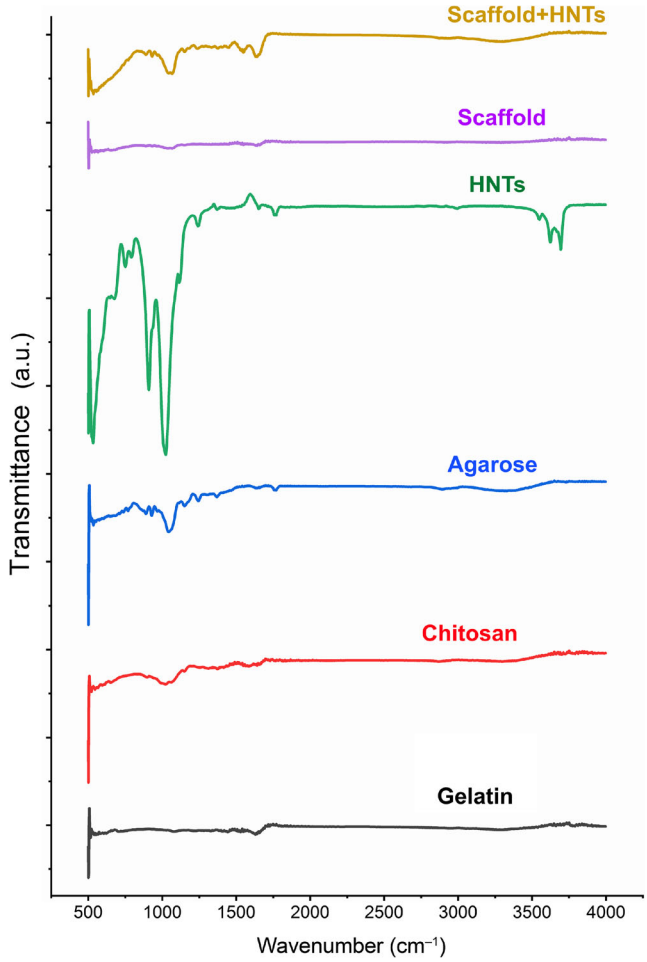

Fig. 2. FTIR spectra of pure polymers, HNTs, and scaffolds

the scaffold appeared to be related to the presence of other biopolymers. The peaks related to the main material (agarose) were present in scaffold samples. Clearly, some shifting in the peak position in the biopolymer matrix indicate formation of the polyelectrolyte complex without addition of reinforcing substances as also described by Kulig et al. (2016) for chitosan and alginate. Generally, the wavenumber range between 87 cm^{-1} and 1300 cm^{-1} in scaffold samples can be considered as a fingerprint region for agarose.

Cells obtained from the dog adipose tissue had the characteristic morphology of MSCs (Fig. 4a, c, d). During the cultivation time (72 h), MSCs on 3D porous matrix doped with HNTs formed spheroid-like structures spontaneously which were further attached to the surface of the matrix (Fig. 4b). This phenomenon demonstrated the ability of MSCs to form tissue-like constructs within the porous gelatine-chitosan-

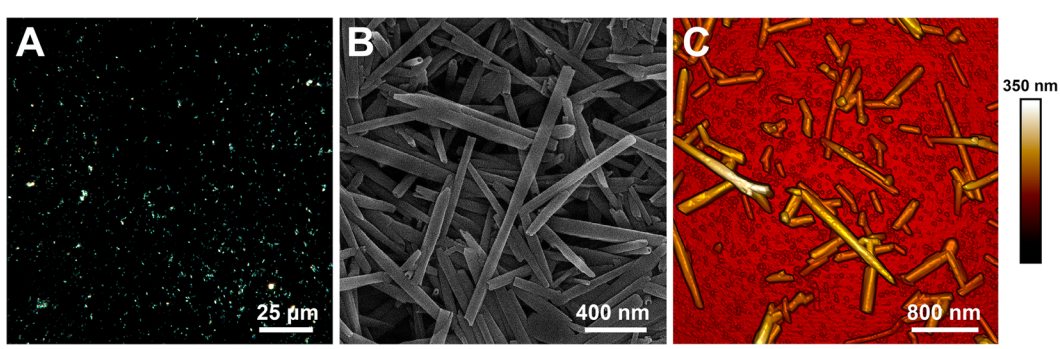

Fig. 3. Visualization of halloysite nanotubes using **a** dark field microscopy, **b** scanning electron microscopy, and **c** atomic force microscopy

https://doi.org/10.1007/s42860-021-00152-7 Published online by Cambridge University Press

agarose scaffold with 6 wt.% of HNTs. Cells in spheroids are not uniform in their physiology, which corresponds more to the state of cells in the natural tissue (Lin & Chang, 2008). Interaction of cells with their neighboring cells and extracellular matrix are also associated with modified diffusion speed (Achili et al., 2012; Rozhina et al., 2019) All of these conditions promote the formation of tissue-mimicking structure from MSCs with high differentiation potential, which is manifested in the corresponding microenvironment in the presence of specific factors.

Using immunocytochemical staining and fluorescent microscopy analysis, cells isolated from adipose tissue of a dog have been shown to act as markers of MSCs (CD 44, CD 10, CD 71) (Fig. 5).

To determine the differentiation potential of the isolated cells, the specific media containing the growth factors which transform cells into specialized cells were used. Subsequent staining for specific products indicated the differentiation potential of MSCs in three directions (with relevant controls which had no specific growth factors): osteogenic (Fig. 6a, d), chondrogenic (Fig. 6b, e), and adipogenic (Fig. 6c, f).

The opportunity for MSCs to differentiate in the osteogenic direction was examined on the surface of native polymeric matrices and nanostructured scaffolds with 6 wt.% of HNTs (Fig. 7). Osteogenic differentiation of MSCs was observed on the nanostructured matrix material surface (Fig. 7e, f) after 14 days. In the case of a native scaffold, it probably takes more time; after 14 days, only modest morphological changes in cells were noted. The addition of halloysite imparts osteoconductive properties to the matrix material, therefore.

Using AFM, Young's modulus (DMT model) was shown to be greater in the case of osteodifferentiation on the scaffold with HNTs than in the same case but without nanomodification (Table 1). On the other hand, cells and extracellular space on the control scaffold without HNTs and a medium without osteogenic factors were stiffer than those grown on the unmodified matrices. This observation was related to the stage of differentiation process.

Porous biodegradable hydrogel scaffolding doped with nanoparticles can be used, therefore, not only as a passive carrier for stem cells for cell therapy, but also as a conductive material for the formation of tissue-like structures.

In one clinical case example, a 5 year-old Kurtshaar dog (male, body weight 30 kg) was operated on. This dog had a burdened anamnesis according to its owner: a year previously the dog had been injured (a closed comminuted diaphyseal fracture of the left humerus bone) in a traffic accident and was operated on as in the above-mentioned pathological process. A bone osteosynthesis with overlapping of the plate was performed. After 1 month, the rejection of the fixation construction began; the plate was removed and replaced with Kirshner wires. After another 30 days, the rejection of the Kirshner wires began, which were removed before the required time

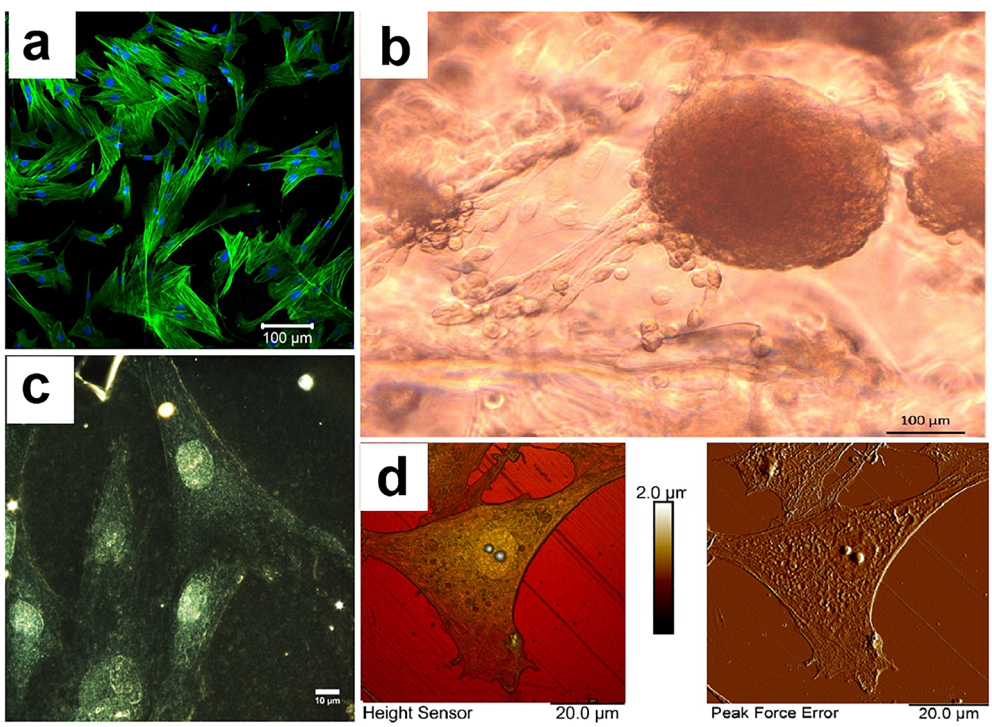

Fig. 4. Morphology and cytoskeleton (F-actin) of allogenic MSCs (6th passage) obtained from **a** dog adipose tissue; **b** growth of dog MSCs on 3D porous biopolymer matrix doped with HNTs; note the spontaneous formation of 3D cell clusters – spheroids; **c**dark-field microscopy image of dog MSCs monolayer; and **d**atomic-force images of single MSC

https://doi.org/10.1007/s42860-021-00152-7 Published online by Cambridge University Press

but the screw remained in the leg (Fig. 8a) and was probably the cause of the hypersensitivity and sensitization.

Thus, the function of the left thoracic limb was impaired and this was manifested by intermittent, strong-degree lameness; a breach of skin integrity and pain during palpation were absent; mobility outside the joint, atrophy of extensor muscles and flexors of the elbow joint were noted. During the operation, the foreign body (screw) was removed, and the granulation tissue surrounding the fracture zone was excised. Complete repositioning of fragments was not achieved due to contracture of the elbow joint. A porous biopolymer matrix with allogenic dog MSCs was placed between the ends of the fragments. Fixation of the fragments was performed by retrograde fitting of two Kirschner wires with a diameter of 3 mm. Additional immobilization was provided by the application of the SoftCast bandage.

Clinical blood tests were within the normal range before and after the operation, but a slight degree of anaemia arose (Table 2).

At the 7th day after surgery, a radiographic examination was performed (Fig. 8b). The fracture line on the roentgenogram was fuzzy, pronounced periosteal reaction along the bone length was observed, and the cortical layer was thinned and indistinct. Then, 30 days after the operative intervention, a periosteal corn bounded by a zone of fracture was formed, the fracture line was not clear, the lower fragment was osteoporotic, and an intermittent endosteal callus formed on the posterior surface of the bone (Fig. 8c).

In general, the course of the post-operative period was favorable, but after a month, the Kirshner wires had to be removed due to the development of oedema. Infusion with saline was performed. After the removal of the Kirshner wires, the general state of the dog improved and the oedema decreased. Blood analysis revealed an increase in the level of alkaline phosphatase and stab neutrophils, which is probably an indicator of an allergic reaction due to individual intolerance to metals (Tables 3, 4).

Finally, the removal of the Kirshner wires led to the normalization of the limb state; the dog began to use the limb during walking. The use of porous biopolymer matrix together with stem cells contributed to a more active formation of bone callus and fracture fusion, which was not achieved during the previous operation using only metal-supporting constructions.

DISCUSSION

In general, regeneration of bone is a much slower process than repair of bone defects. Several key factors have been identified for the successful repair of bone: the defect zone must be fully occupied by the implant material to inhibit

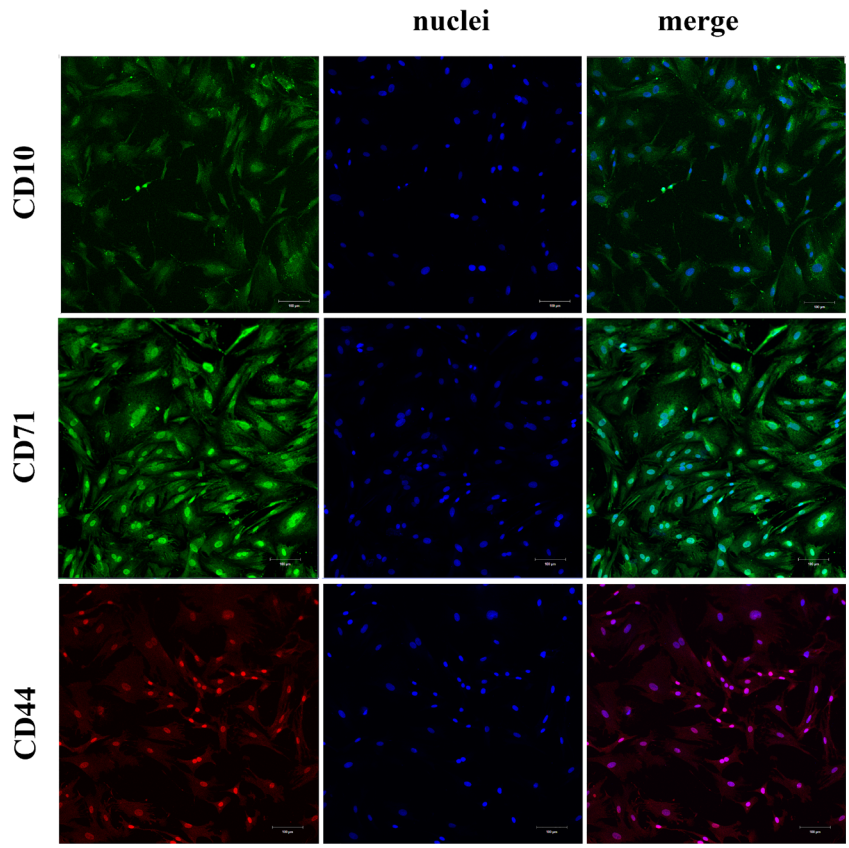

Fig. 5. Positive staining of MSCs on stem-cells markers (CD10, CD71, CA44). Scale bar = 100 μm

https://doi.org/10.1007/s42860-021-00152-7 Published online by Cambridge University Press

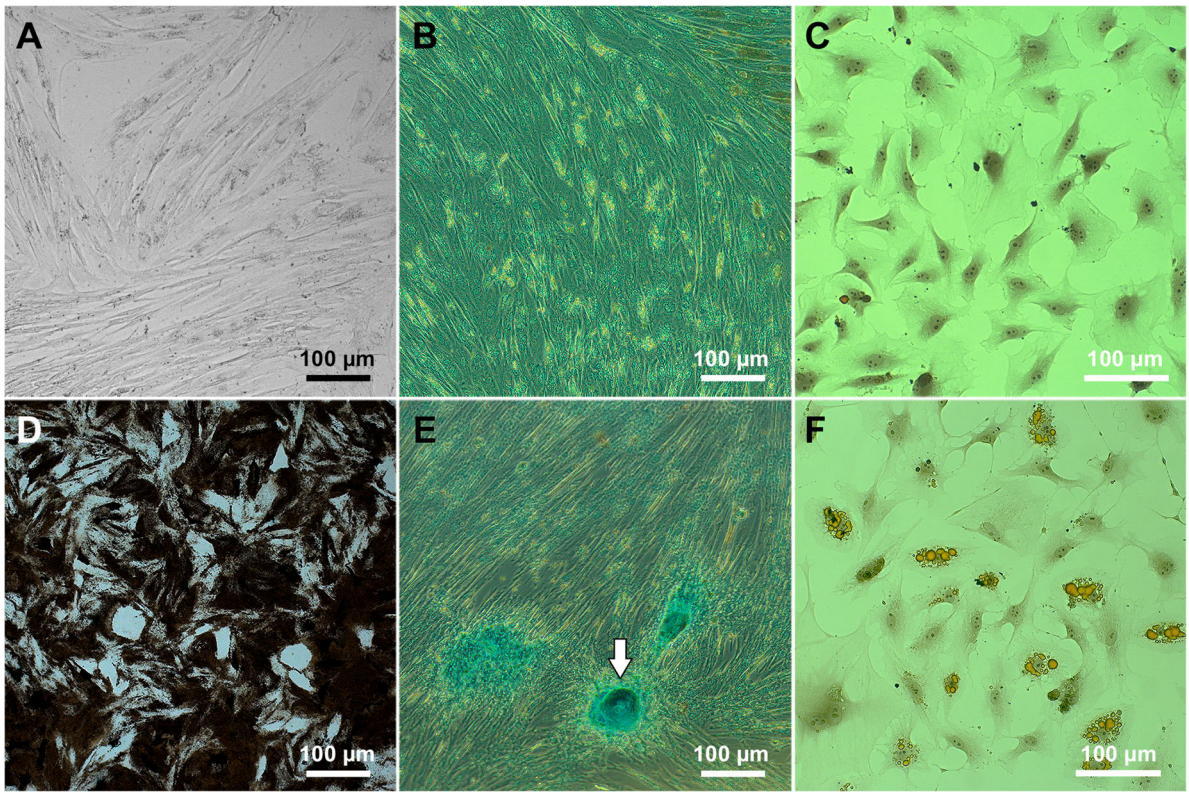

Fig. 6. Differentiation of MSCs: **a**, **b**, **c** control (cells grown without specific growth factors); **d** cells grown in osteogenic differentiation medium (von Kossa staining; black color indicates the mineralization zones); **e** cells grown in chondrogenic differentiation medium (Alcian blue staining; white arrow marks the cartilage formation zone with blue-colored acid mucopolysaccharides); and **f** cells, grown in adipogenic differentiation medium, Sudan 3 staining (note the oil drops inside the cells)

dysfunctional fibrosis; MSCs must migrate into or be placed within the boundaries of the bone defect; these boundaries must be occupied by a cell-delivery vehicle that either is resorbed or becomes functionally integrated into the new structure. Several varieties of biomaterials have been studied and used clinically for bone repair and regeneration applications (Dimitriou et al., 2011; Tan et al., 2013; Ou et al., 2020; Pereira et al., 2020).

A previous study demonstrated that stem-cell therapy accelerated the bone-defect regeneration that was effective for the treatment of osteonecrosis of the femoral head in the complex therapy (Wu et al., 2020). A combination of allogeneic and autogenous MSCs with scaffolds on the base of fibrinogen and collagen demonstrated the efficacy of cell-based therapies for the treatment of bone defects by growth of newly formed cartilaginous tissue at the site of the original physeal defect (Planka et al., 2008). As demonstrated by Song et al. (2020), highly aligned, fullerene nanowhisker, nanopatterned surfaces contribute to the preservation of multipotency and enhance regenerative capacity in MSCs. Soft scaffolds mimicking extracellular matrix on the base of fibronectin were fabricated by Jia et al. (2020). These scaffolds represent tunable adaptive materials, composed of a protein monolayer assembled at a liquid–liquid interface, which adapt dynamically to cell-traction forces and can influence the stem-cell differentiation and enable dynamic control of stem-cell behavior. Using Von Kossa staining methods and AFM in the present study, the ability of dog MSCs to differentiate in an osteogenic direction on the surface of hydrogels doped with HNTs under osteogenic conditions was noted. AFM was also used to determine alteration in the stiffness and elasticity of samples during osteodifferentiation. To find the Young's modulus of a surface, selecting a suitable model of the mechanics of contact between the AFM probe and the sample surface is necessary. The most commonly used models were developed by Hertz (1881), Johnson-Kendall-Roberts (JKR) (Johnson et al., 1971), and Derjaguin-Mueller-Toporov (DMT) (Derjaguin et al., 1975). The DMT model was chosen; this refines the simplest model (Hertz), taking into account adhesion outside the contact area, and is more applicable to small cantilevers (Bruker ScanAsyst-Air probes, Billerica, Massachusetts, Bruker, USA) (nominal length 115 μm, tip radius 2 nm, spring constant 0.4 Nm^{-1})) in contact with rigid specimens with low adhesion (Heinz & Hoh, 1999).

In previous studies by the current authors, combinations of natural biopolymers, chitosan, agarose, gelatin, and hyaluronic acid were used to produce porous tissue engineering scaffolds. These biopolymer compositions were doped with

https://doi.org/10.1007/s42860-021-00152-7 Published online by Cambridge University Press

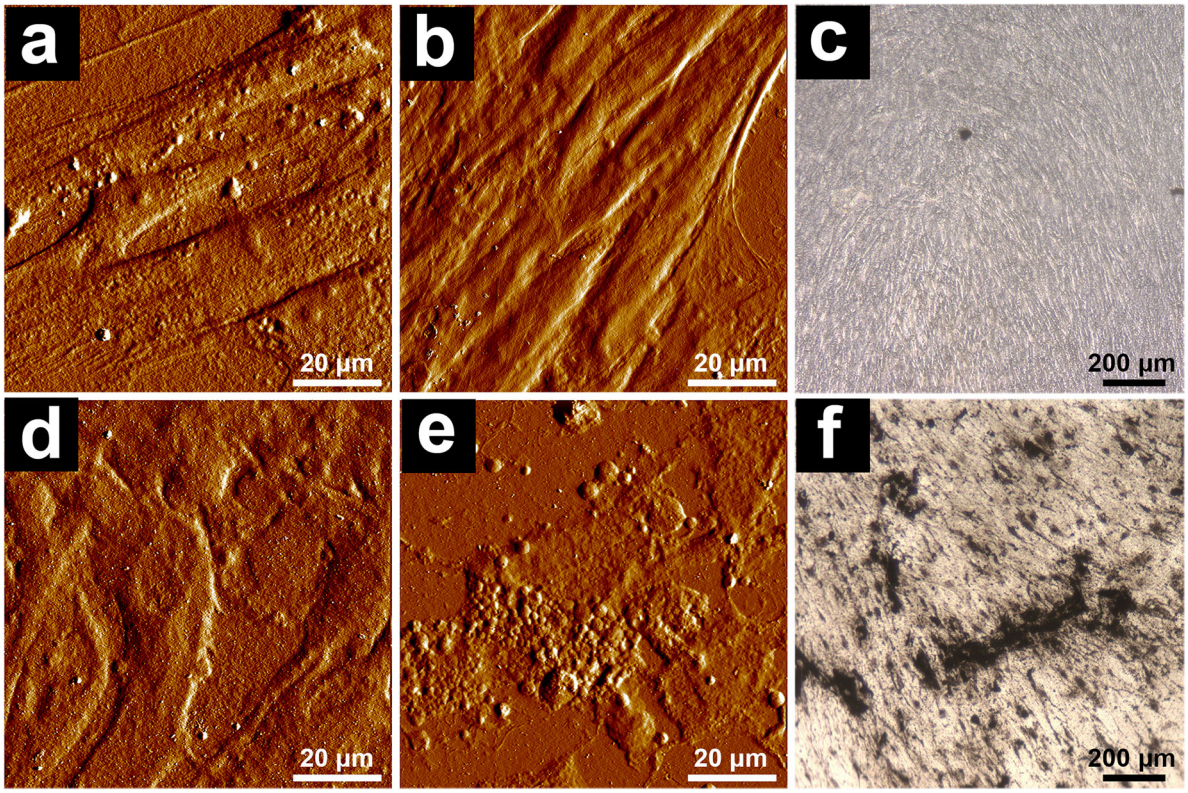

Fig. 7. Osteodifferentiation of MSCs on the biopolymer scaffolds. **a** control cells grown on α-MEM on the scaffold without HNTs; **b** control cells grown on α-MEM on the scaffold with 6 wt.% HNTs; **c** von Kossa staining of cells grown on α-MEM on the scaffold with 6 wt.% HNTs; **d** cells grown on osteodifferentiation cultural medium on the scaffold without HNTs; **e** cells grown on osteodifferentiation cultural medium on the scaffold with 6 wt.% HNTs; and **f** von Kossa staining of cells grown on osteodifferentiation cultural medium on the scaffold with 6 wt.% HNTs

natural nanofiller (halloysite nanotubes) to enhance both the biological compatibility and the mechanical properties of scaffolds (Suner et al., 2019; Naumenko & Fakhrullin, 2019). The surface irregularities of the scaffold pores due to the insoluble nanotubes promoted the best adhesion of the cells on scaffold materials. Moreover, they increased the strength of the composites. HNTs have been used successfully in several studies as nanomodifiers (Sun et al., 2010; Zheng & Wang, 2010; de Silva et al., 2013; Okamoto & John, 2013; Liu et al., 2013) and showed no significant toxicity. Previous work (Naumenko et al., 2016) demonstrated that the addition of even small amounts of nanofiller (3–6 wt.%) led to significant improvement in mechanical stability and wettability of the biopolymer scaffolds and did not disturb the cell growth in vitro. In vivo study has demonstrated the biocompatibility of nanocomposite scaffolds studied in the organisms of rats, with a slight inflammatory effect but without rejection of implants. The approximate period of degradation was ~6 weeks, which was confirmed by histological examination. The blood supply of the implanted area was restored fully in six weeks. On the other hand, the addition of a significant amount of HNTs (up to 50 wt.%) to biopolymer matrix did not disturb the cell proliferation and hemocompatibility (Suner et al., 2019). Data obtained in the present study as well as in previous experiments suggest that the HNTs-modified biopolymer composites show great potential in tissue engineering and can be used as stem-cell carriers for bone repair in vivo.

Table 1. Mechanical characteristics of cells and extracellular space after osteogenic differentiation (14 days)

Control – HNT		control + HNT		Osteo – HNT		Osteo + HNT	
Adhesion (nN)	Modulus (MPa)	Adhesion (nN)	Modulus (MPa)	Adhesion (nN)	Modulus (MPa)	Adhesion (nN)	Modulus (MPa)
1e3.1±0.9	250.9±64.9	4.8±1.8	78.4±7.9	4.3±0.4	38.7±5.3	2.6±1.4	317.6±54.3

https://doi.org/10.1007/s42860-021-00152-7 Published online by Cambridge University Press

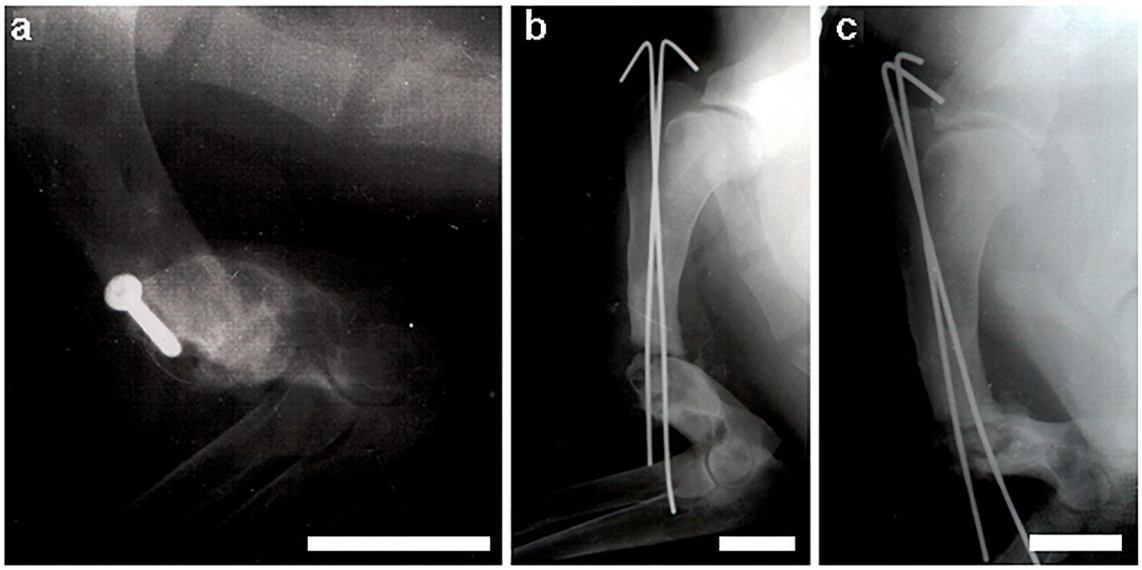

Fig. 8. X-ray images of the damaged limb: **a** complete chronic diaphyseal fracture of the left humerus with an offset at an angle complicated by neoarthrosis and athrogenic elbow joint contracture; note a foreign body in the area of the proximal fragment (fixation screw). **b** the state of the limb 7 days after the operation, and **c** 30 days after the operation. Scale bar = 5 cm

Table 2. Change of main hematological parameters in the early post-operative period

Terms	Parameters		
	Erythrocytes (10^{12}/L)	Hemoglobin (g/L)	Erythrocyte sedimentation rate (mm/h)
Before operation	6.9	138	4
After 7 days	6.2	144	5

Table 3. Changes in Leukogram in the early postoperative period

Parameters		Terms	
		Before operation	After 7 days
Leucocytes (10^9/L)		19.9	20
Eosinophils (%)		10	21.3
Basophils (%)		–	1
Neutrophils (%)	Stab-nuclear	20	–
	Segmented-nuclear	47	28
Lymphocytes (%)		20	50
Monocytes (%)		3	18

Table 4. Changes in biochemical parameters of blood serum in the early post-operative period

Terms	Parameters				
	Total protein (g/L)	Alkaline phosphatase (U/L)	Total Ca (mM/L)	Inorganic P (mM/L)	C-reactive Protein
Before operation	80	76	2.09	1.08	+
After 7 days	54	103	2.28	1.5	–

https://doi.org/10.1007/s42860-021-00152-7 Published online by Cambridge University Press

CONCLUSIONS

The use of biopolymer matrices in combination with stem cells promoted normal regeneration of bone tissue even in the case of complex fractures with incorrect primary fusion of bones. In addition, manifestations of rejection were observed. The bones of an animal prone to allergic reaction to metals were regenerated more efficiently after the removal of metal constructs; due to the lack of fixing time, however, the bone was displaced in the area of the callus formed. No inflammatory reaction was observed with respect to the nanocomposite biopolymer matrix and allogenic MSC. The combination of traditional surgery using metallic constructions with implantation of 3D-biopolymeric matrices can be effective in terms of bone regeneration.

ACKNOWLEDGMENTS

The present study was funded by the Russian Foundation for Basic Research (project number 20-015-00353) and partially supported by RFBR and the government of the Tatarstan Republic (grant number 18-415-160010).

FUNDING

Funding sources are as stated in the Acknowledgments.

Declarations

Conflict of Interest

The authors declare that they have no conflict of interest.

REFERENCES

Abdullayev, E., & Lvov, Y. (2013). Halloysite clay nanotubes as a ceramic "skeleton" for functional biopolymer composites with sustained drug release. *Journal of Materials Chemistry B, 1*, 2894–2903.

Achili, T.-M., Meyer, J., & Morgan, J. R. (2012). Advances in the formation, use and understanding of multicellular spheroids. *Expert Opinion on Biological Therapy, 12*(*10*), 1347–1360.

Akhatova, F., Danilushkina, A., Kuku, G., Saricam, M., Culha, M., & Fakhrullin, R. (2018a). Simultaneous intracellular detection of plasmonic and non-plasmonic nanoparticles using dark-field hyperspectral microscopy. *Bulletin of the Chemical Society of Japan, 91*(*11*), 1640–1645.

Akhatova, F., Fakhrullina, G., Khakimova, E., & Fakhrullin, R. (2018b). Atomic force microscopy for imaging and nanomechanical characterisation of live nematode epicuticle: A comparative Caenorhabditis elegans and Turbatrix aceti study. *Ultramicroscopy, 194*, 40–47.

Alstrup, T., Eijken, M., Bohn, A. B., Møller, B., & Damsgaard, T. E. (2019). Isolation of adipose tissue-derived stem cells: enzymatic digestion in combination with mechanical distortion to increase adipose tissue-derived stem cell yield from human aspirated fat. *Current Protocols in Stem Cell Biology, 48*(*1*), e68.

Athanasiou, K. A., Zhu, C., Lanctot, D. R., Agrawal, C. M., & Wang, X. (2000). Fundamentals of biomechanics in tissue engineering of bone. *Tissue Engineering, 6*, 361–381.

Bertesteanu, S., Chifiriuc, M. C., Grumezescu, A. M., Printza, A. G., Marie-Paule, T., Grumezescu, V., Michaela, V., Lazar, V., & Grigore, R. (2014). Biomedical applications of synthetic, biodegradable polymers for the development of anti-infective strategies. *Current Medicinal Chemistry, 21*(*29*), 3383–3390.

Blokhuis, T. J. (2014). Bioresorbable bone graft substitutes. In K. Mallick (Ed.), *Bone Substitute Biomaterials*. Woodhead Publishing Series in Biomaterials (pp. 80–92). Elsevier.

Cavalcanti, S. C., Pereira, C. L., Mazzonetto, R., de Moraes, M., & Moreira, R. W. (2008). Histological and histomorphometric analyses of calcium phosphate cement in rabbit calvaria. *Journal of Cranio-Maxillofacial Surgery, 36*, 354–359.

Cavallaro, G., Milioto, S., Konnova, S., Fakhrullina, G., Akhatova, F., Lazzara, G., Fakhrullin, R., & Lvov, Y. (2020). Halloysite/Keratin nanocomposite for human hair photoprotection coating. *ACS Applied Materials & Interfaces, 12*, 24348–24362.

Cho, J. S., Park, J. H., Kang, J. H., Kim, S. E., Park, I. H., & Lee, H. M. (2015). Isolation and characterization of multipotent mesenchymal stem cells in nasal polyps. *Experimental Biology and Medicine (Maywood, N.J.), 240*(*2*), 185–193.

Christensen, F. B., Dalstra, M., Sejling, F., Overgaard, S., & Bunger, C. (2000). Titanium-alloy enhances bone-pedicle screw fixation: Mechanical and histomorphometrical results of titanium-alloy versus stainless steel. *European Spine Journal, 9*, 97–103.

Cornell, C. N. (1999). Osteoconductive materials and their role as substitutes for autogenous bone grafts. *Orthopedic Clinics of North America, 4*, 591–598.

Curtis, R., Goldhahn, J., Schwyn, R., Regazzoni, P., & Suhm, N. (2005). Fixation principles in metaphyseal bone—A patent based review. *Osteoporosis International, 16*, S54–S64.

de Silva, R. T., Pasbakhsh, P., Goh, K. L., Chai, S.-P., & Ismail, H. (2013). Physico-chemical characterisation of chitosan/halloysite composite membranes. *Polymer Testing, 32*, 265–271.

Derjaguin, B. V., Muller, V. M., & Toporov, Y. P. (1975). Effect of contact deformations on the adhesion of particles. *Journal of Colloid and Interface Science, 53*, 314–326.

Dimitriou, R., Jones, E., Mcgonagle, D., & Giannoudis, P. V. (2011). Bone regeneration: current concepts and future directions. *BMC Medicine, 9*, 66.

Driessens, F. C., van Dijk, J. W., & Borggreven, J. M. (1978). Biological calcium phosphates and their role in the physiology of bone and dental tissues I. Composition and solubility of calcium phosphates. *Calcified Tissue International, 26*, 127–137.

Eppley, B. L., & Sadove, A. M. (1995). A comparison of resorbable and metallic fixation in healing of calvarial bone grafts. *Plastic and Reconstructive Surgery, 96*, 316–322.

Fakhrullina, G. I., Akhatova, F. S., Lvov, Y. M., & Fakhrullin, R. F. (2015). Toxicity of halloysite clay nanotubes in vivo: a Caenorhabditis elegans study. *Environmental Science: Nano, 2*, 54–59.

Fakhrullina, G., Akhatova, F., Kibardina, M., Fokin, D., & Fakhrullin, R. (2017). Nanoscale imaging and characterization of Caenorhabditis elegans epicuticle using atomic force microscopy. *Nanomedicine: Nanotechnology, Biology and Medicine, 13*(*2*), 483–491.

Fakhrullina, G., Khakimova, E., Akhatova, F., Lazzara, G., Parisi, F., & Fakhrullin, R. F. (2019). Selective antimicrobial effects of curcumin@halloysite nanoformulation: a Caenorhabditis elegans study. *ACS Applied Materials & Interfaces, 11*(*26*), 23050–23064.

Glotov, A., Stavitskaya, A., Chudakov, Y., Ivanov, E., Huang, W., Vinokurov, V., Zolotukhina, A., Maximov, A., Karakhanov, E., & Lvov, Y. (2019). Mesoporous metal catalysts templated on clay nanotubes. *Bulletin of the Chemical Society of Japan, 92*(*1*), 61–69.

Goodrich, J. T., Sandler, A. L., & Tepper, O. (2012). A review of reconstructive materials for use in craniofacial surgery bone fixation materials, bone substitutes, and distractors. *Child's Nervous System, 28*, 1577–1588.

Guryanov, I., Naumenko, E., Akhatova, F., Nigamatzyanova, L., & Fakhrullin, R. (2020). Selective cytotoxic activity of prodigiosin@halloysite nanoformulation. *Frontiers in Bioengineering and Biotechnology, 8*, 424.

Heinz, W. F., & Hoh, J. H. (1999). Spatially resolved force spectroscopy of biological surfaces using the atomic force microscope. *Trends in Biotechnology, 17*, 143–150.

Hertz, H. (1881). Über die Berührung fester elastischer Körper. *Journal für die reine und angewandte Mathematik, 92*, 156–171.

Hutmacher, D., Hurzeler, M. B., & Schliephake, H. (1996). A review of material properties of biodegradable and bioresorbable polymers and devices for GTR and GBR applications. *The International Journal of Oral & Maxillofacial Implants, 11*, 667–678.

Jia, X., Minami, K., Uto, K., Chang, A. C., Hill, J. P., Nakanishi, J., & Ariga, K. (2020). Adaptive liquid interfacially assembled protein nanosheets for guiding mesenchymal stem cell fate. *Advanced Materials, 32*, 1905942.

Johnson, K. L., Kendall, K., & Roberts, A. D. (1971). Surface energy and the contact of elastic solids. *Proceedings of the Royal Society of London A. Mathematical and Physical Sciences, 324*, A324301–A324313.

Kulig, D., Zimoch-Korzycka, A., Jarmoluk, A., & Marycz, K. (2016). Study on alginate–chitosan complex formed with different polymers ratio. *Polymers, 8*(5), 167.

Lin, R.-Z., & Chang, H.-Y. (2008). Recent advances in three-dimensional multicellular spheroid culture for biomedical research. *Biotechnology Journal, 3*, 1172–1184.

Liu, M., Wu, C., Jiao, Y., Xiong, S., & Zhou, C. (2013). Chitosan–halloysite nanotubes nanocomposite scaffolds for tissue engineering. *Journal of Materials Chemistry B, 1*, 2078–2089.

Lo Furno, D., Graziano, A. C., Caggia, S., Perrotta, R. E., Tarico, M. S., Giuffrida, R., & Cardile, V. (2013). Decrease of apoptosis markers during adipogenic differentiation of mesenchymal stem cells from human adipose tissue. *Apoptosis: an International Journal on Programmed Cell Death, 18*(5), 578–588.

Marti, C., Imhoff, A. B., Bahrs, C., & Romero, J. (1997). Metallic versus bioabsorbable interference screw for fixation of bone-patellar tendon-bone autograft in arthroscopic anterior cruciate ligament reconstruction. A preliminary report. *Knee Surgery, Sports Traumatology, Arthroscopy, 5*, 217–221.

Meloan, S. N., & Puchtler, H. (1985). Chemical mechanisms of staining methods: von Kossa's technique: What von Kossa really wrote and a modified reaction for selective demonstration of inorganic phosphates. *Journal of Histotechnology, 8*(*1*), 11–13.

Middleton, J. C., & Tipton, A. J. (2000). Synthetic biodegradable polymers as orthopedic devices. *Biomaterials, 21*, 2335–2346.

Naumenko, E. A., & Fakhrullin, R. F. (2017). Toxicological evaluation of clay nanomaterials and polymer-clay nanocomposites. In Y. M. Lvov, B. Guo, & R. F. Fakhrullin (Eds.), *Functional Polymer Composites with Nanoclays* (pp. 399–419). Royal Society of Chemistry.

Naumenko, E., & Fakhrullin, R. (2019). Halloysite nanoclay/biopolymers composite materials in tissue engineering. *Biotechnology Journal, 14*(*12*), 1900055.

Naumenko, E. A., Guryanov, I. D., Yendluri, R., Lvov, Y. M., & Fakhrullin, R. F. (2016). Clay nanotube–biopolymer composite scaffolds for tissue engineering. *Nanoscale, 8*, 7257–7271.

Okamoto, M., & John, B. (2013). Synthetic biopolymer nanocomposites for tissue engineering scaffolds. *Progress in Polymer Science, 38*, 1487–1503.

Ou, Q., Huang, K., Fu, C., Huang, C., Fang, Y., Gu, Z., Wu, J., & Wang, Y. (2020). Nanosilver-incorporated halloysite nanotubes/gelatin methacrylate hybrid hydrogel with osteoimmunomodulatory and antibacterial activity for bone regeneration. *Chemical Engineering Journal, 382*, 123019.

Pereira, H. F., Cengiz, I. F., Silva, F. S., Reis, R. L., & Oliveira, J. M. (2020). Scaffolds and coatings for bone regeneration. *Journal of Materials Science: Materials in Medicine, 31*(*3*), 27.

Planka, L., Gal, P., Kecova, H., Klima, J., Hlucilova, J., Filova, E., Amler, E., Krupa, P., Kren, L., Srnec, R., Urbanova, L., Lorenzova, J., & Necas, A. (2008). Allogeneic and autogenous transplantations of MSCs in treatment of the physeal bone bridge in rabbits. *BMC Biotechnology, 8*, 70.

Rabie, A. B., Wong, R. W., & Hagg, U. (2000). Composite autogenous bone and demineralized bone matrices used to repair defects in the parietal bone of rabbits. *British Journal of Oral and Maxillofacial Surgery, 38*, 565–570.

Rozhina, E., Batasheva, S., Gomzikova, M., Naumenko, E., & Fakhrullin, R. (2019). Multicellular spheroids formation: The synergistic effects of halloysite nanoclay and cationic magnetic nanoparticles. *Colloids and Surfaces A: Physicochemical and Engineering Aspects, 565*, 16–24.

Rozhina, E., Panchal, A., Akhatova, F., Lvov, Y., & Fakhrullin, R. (2020). Cytocompatibility and cellular uptake of alkylsilane-modified hydrophobic halloysite nanotubes. *Applied Clay Science, 185*, 105371.

Shall, G., Menosky, M., Decker, S., Nethala, P., Welchko, R., Leveque, X., Lu, M., Sandstrom, M., Hochgeschwender, U., Rossignol, J., & Dunbar, G. (2018). Effects of passage number and differentiation protocol on the generation of dopaminergic neurons from rat bone marrow-derived mesenchymal stem cells. *International Journal of Molecular Sciences, 19*(3), 720.

Singh, R., Bhattacharya, B., Tomar, S. K., Singh, V., & Singh, P. K. (2017). Electrical, optical and electrophotochemical studies on agarose based biopolymer electrolyte towards dye sensitized solar cell application. *Measurement, 102*, 214–219.

Song, J., Jia, X., Minami, K., Hill, J. P., Nakanishi, J., Shrestha, L. K., & Ariga, K. (2020). Large-area aligned fullerene nanocrystal scaffolds as culture substrates for enhancing mesenchymal stem cell self-renewal and multipotency. *ACS Applied Nano Materials, 3*, 6497–6506.

Sun, X. M., Zhang, Y. H., Shen, B., & Jia, N. Q. (2010). Direct electrochemistry and electrocatalysis of horseradish peroxidase based on halloysite nanotubes/chitosan nanocomposite film. *Electrochimica Acta, 56*(*2*), 700–705.

Suner, S. S., Demirci, S., Yetiskin, B., Fakhrullin, R., Naumenko, E., Okay, O., Ayyala, R. S., & Sahiner, N. (2019). Cryogel composites based on hyaluronic acid and halloysite nanotubes as scaffold for tissue engineering. *International Journal of Biological Macromolecules, 130*, 627–635.

Tan, L., Yu, X., Wan, P., & Yang, K. (2013). Biodegradable materials for bone repairs: A review. *Journal of Materials Science & Technology, 29*, 503–513.

Tarasova, E., Naumenko, E., Rozhina, E., Akhatova, F., & Fakhrullin, F. (2019). Cytocompatibility and uptake of polycations-modified halloysite clay nanotubes. *Applied Clay Science, 169*, 21–30.

Ulery, B. D., Nair, L. S., & Laurencin, C. T. (2011). Biomedical applications of biodegradable polymers. *Journal of Polymer Science Part B: Polymer Physics, 49*, 832–864.

Wu, Z. Y., Sun, Q., Liu, M., Grottkau, B. E., He, Z. X., Zou, Q., & Ye, C. (2020). Correlation between the efficacy of stem cell therapy for osteonecrosis of the femoral head and cell viability. *BMC Musculoskeletal Disorders, 21*, 55.

Wuisman, P. I., & Smit, T. H. (2006). Bioresorbable polymers: Heading for a new generation of spinal cages. *European Spine Journal, 15*, 133–148.

Yang, Y.-H. K., Ogando, C. R., Wang See, C., Chang, T.-Y., & Barabino, G. A. (2018). Changes in phenotype and differentiation potential of human mesenchymal stem cells aging in vitro. *Stem Cell Research & Therapy, 9*, 131. https://doi.org/10.1186/s13287-018-0876-3

Yendluri, R., Lvov, Y., de Villiers, M. M., Vinokurov, V., Naumenko, E., Tarasova, E., & Fakhrullin, R. (2017). Paclitaxel encapsulated in halloysite clay nanotubes for intestinal and intracellular delivery. *Journal of Pharmaceutical Sciences, 106*(10), 3131–3139.

Zheng, Y., & Wang, A. (2010). Enhanced adsorption of ammonium using hydrogel composites based on chitosan and halloysite. *Journal of Macromolecular Science Part A Pure and Applied Chemistry, 47*(*1*), 33–38.

(Received 28 April 2021; Revised 9 August 2021; AE: J.W. Stucki)